(3) Sundararajan, P. R.; Tyrer, N. J.; Bluhm, T. L. *Macromolecules* **1982**, *15*, 286.
(4) Guenet, J. M. *Macromolecules* **1986**, *19*, 1961.
(5) Perez, E.; Vanderhart, D. L.; McKenna, G. B. *Macromolecules* **1988**, *21*, 2418.
(6) Guenet, J. M. *Macromolecules* **1987**, *20*, 2874.
(7) Guenet, J. M.; McKenna, G. B. *Macromolecules* **1988**, *21*, 1752.
(8) Natta, G. *J. Polym. Sci.* **1955**, *16*, 143.
(9) Guenet, J. M.; Gallot, Z.; Picot, C.; Benoit, H. *J. Appl. Polym. Sci.* **1977**, *21*, 2181.
(10) Atkins, E. D. T.; et al. *Colloid Polym. Sci.* **1984**, *262*, 22.
(11) Bellissent, R.; Chenevas-Paule, A.; Roth, M. *J. Non-Cryst. Solids* **1983**, *59-60*, 229.
(12) See, for instance: Guinier, A. In *Théorie et Technique de la Radiocristallographie*; Dunod: Paris, 1955.
(13) Natta, G.; Corradini, P.; Bassi, I. W. *Suppl. Nuovo Cimento* **1960**, *15*, 68.
(14) Watanabe, J.; Sasanuma, Y.; Endo, A.; Uematsu, I. *Rep. Prog. Polym. Phys. Jpn.* **1980**, *23*, 667.
(15) He, X.; Herz, J.; Guenet, J. M. *Macromolecules* **1987**, *20*, 2003.
(16) Zimm, B. H. *J. Chem. Phys.* **1948**, *16*, 1093.
(17) Daoud, M.; et al. *Macromolecules* **1975**, *8*, 804.
(18) Sadler, D. M.; Keller, A. *Macromolecules* **1977**, *10*, 1128.
(19) Guenet, J. M. *Macromolecules* **1980**, *13*, 380.
(20) Guenet, J. M. *Polymer* **1981**, *22*, 313.
(21) Yoshisaki, T.; Yamakawa, H. *Macromolecules* **1980**, *13*, 1518.
(22) Muroga, Y. *Macromolecules* **1988**, *21*, 2751.
(23) Hermans, J.; Hermans, J. J. *J. Phys. Chem.* **1958**, *62*, 1543.
(24) McKenna, G. B.; Guenet, J. M. *Polym. Commun.* **1988**, *29*, 58.
(25) Rawiso, M.; Duplessix, R.; Picot, C. *Macromolecules* **1987**, *20*, 630.
(26) de Gennes, P.-G. In *Polymer Liquid Crystals*; Academic Press: New York, 1982.
(27) Debye, P.; Bueche, A. M. *J. Appl. Phys.* **1949**, *20*, 518.
(28) Sadler, D. M.; Harris, R. *J. Polym. Sci., Polym. Phys. Ed.* **1982**, *20*, 561.
(29) Talmon, Y.; Prager, S. *J. Chem. Phys.* **1978**, *69*, 2984.
(30) See, for instance: Hoffman, J. D.; Davis, G. T.; Lauritzen, J. I., Jr. In *Treatise on Solid State Chemistry*; Hanney, N. B., Ed.; Plenum: New York; Chapter 7.
(31) Terech, P., private communication, to be submitted.
(32) Heine, S.; Kratky, O.; Porod, G.; Schmitz, J. P. *Makromol. Chem.* **1961**, *44*, 682.
(33) Des Cloizeaux, J. *Macromolecules* **1973**, *6*, 403.
(34) Luzzati, V.; Benoit, H. *Acta Crystallogr.* **1961**, *14*, 297.
(35) Guenet, J. M. *Polymer* **1980**, *21*, 1385.
(36) Porod, G. *Kolloid Z.* **1951**, *124*, 83; **1952**, *125*, 51.

Forces between Surfaces with Adsorbed Polymers. 3. Θ Solvent. Calculations and Comparison with Experiment

Kevin Ingersent,[†] Jacob Klein,*[,‡] and Philip Pincus[§]

Magdalene College, Cambridge, England, Polymer Department, Weizmann Institute of Science, Rehovot 76100, Israel, and Corporate Laboratories, Exxon Research and Engineering Corporation, Clinton Township, Annandale, New Jersey 08801.
Received December 20, 1988; Revised Manuscript Received June 26, 1989

ABSTRACT: The adsorption of polymers onto a surface from a Θ solvent is treated in terms of a mean-field model based on a Cahn–de Gennes approach. In particular, we calculate the forces between two such polymer bearing surfaces and compare our results in some detail with available experimental data on force profiles between mica surfaces bearing adsorbed polymer near the Θ temperature. All parameters in our model may be estimated from experiment. The predicted force profiles are in very good qualitative agreement with the experimental data, though the absolute spatial and energy scales are smaller for the calculated profiles by factors of ca. 4 and 2.5 relative to experiment. The causes of this discrepancy and possible improvements to the model are considered.

I. Introduction

The technological importance of colloid stabilization and destabilization (or flocculation) by polymers has resulted in extensive experimental and theoretical studies of polymer adsorption and the resulting force between two coated surfaces; the situation to about 1982 is summarized in comprehensive reviews.[1,2] Generally, the adsorption free energy of a high molecular weight polymer attracted to an interface greatly exceeds thermal energies, leading to a quasi-irreversible attachment; i.e., after a long incubation of a surface in contact with a polymer solution, the solution may be replaced by pure solvent with negligible reduction of the surface excess (in the case of polymers that are very marginally adsorbed, some desorption may occur on washing). When two such surfaces are brought together, the mutual interaction arises from a balance between (attractive) bridging and the increased osmotic polymer–polymer coupling resulting from the augmented concentration between the plates. Thus, it is not surprising that the disjoining pressure is very sensitive to the structure of the segment distribution for adsorbed polymers.

For a single surface, the interfacial structure of adsorbed polymers has been actively investigated in recent years. Theoretically, Scheutjens and Fleer[3] have applied the transfer matrix formalism,[4] in conjunction with a Flory–Huggins free-energy functional for the polymer solution. Bulk polymer solution properties in good solvents often differ appreciably from mean-field results, in close analogy to critical phenomena;[5] in order to ensure compatibility with bulk properties, de Gennes[6] generalized the Cahn approach[7] for interfacial energies to obey correct scaling relations for polymer solutions. The boundary condition at the interface used in this scaling theory for

[†] Magdalene College. Present address: Department of Physics, University of Pennsylvania, Philadelphia, PA 19104.
[‡] Polymer Department, Weizmann Institute of Science, Rehovot 76100, Israel. Incumbent of Herman Mark Chair in Polymer Physics.
[§] Exxon Research and Engineering Corporation. Present address: Department of Materials Science, University of California at Santa Barbara, Santa Barbara, CA 93106.

0024-9297/90/2223-0548$02.50/0

adsorption was subsequently corrected[8] to take into account the singular behavior of the segment concentration profile near an adsorbing wall recently discovered by Eisenriegler, Kremer, and Binder.[9]

A more detailed experimental picture of the interfacial structure is also emerging. Surface tension measurements in polymer solutions in good[10] and Θ solvents[11] provide indirect evidence which is consistent with scaling theory and the proximal exponent.[8,9] Ellipsometry[12] yields the first moment of the distribution.[13] More recently[14] experiments utilizing the coupling of evanescent optical waves with fluorescent tags have probed the internal structure of the deformed boundary layer. For small colloidal particles[15] and micelles[16] with adsorbed polymers, deuteron labeling combined with small-angle neutron scattering is also yielding conformational information for curved surfaces.

In recent years the question of *forces* between two polymer-bearing surfaces has been studied experimentally using the mica technique pioneered by Tabor and coworkers[17] and extended by Israelachvili and coworkers[18] and Klein and co-workers.[19] In these experiments the forces acting across a liquid medium between two atomically smooth solid surfaces, with and without adsorbed polymer layers, are directly measured. The results provide information on interactions at molecular and submolecular surface–surface separations and are thus well suited for comparison with the predictions of theoretical models. Several different systems have been studied, including polymers in poor[19] ($T < \Theta$) and good[20,21] solvent conditions and polymers near Θ conditions[22,23] (polystyrene in cyclohexane and in cyclopentane).

Both the transfer-matrix (Scheutjens and Fleer[3,4]) and the Cahn–de Gennes method[6,7] have been extended to the case of *interaction* between two planar surfaces with adsorbed polymers. Klein and Pincus[24] have used the latter approach to calculate interactions between plates with adsorbed polymer in poor solvent conditions; their model has been solved numerically,[25] and the results have been critically compared with surface force measurements (using the mica method) in the polystyrene–cyclohexane system under worse than Θ conditions.

In this paper, we extend the Cahn[6]–de Gennes[7] approach to solve for the interaction between polymer-bearing surfaces in a Θ solvent and compare our calculated predictions with the results of the mica experiments. In particular we investigate how the interaction varies with surface separation and with the excess of adsorbed polymer on the surfaces.

In section II we consider the adsorption profiles for a single plate in a polymer solution at Θ conditions, both before and after washing with pure solvent, and in section III the equations determining the interaction between two such polymer-bearing surfaces are derived. These are solved using a numerical procedure briefly described in section IV, and the results are presented in section V. In section VI the theoretical force–distance curves are critically compared with the experimental profiles, and in section VII we make some concluding remarks.

II. Single Plate Profile

Our approach in this paper is similar to that described by de Gennes[6] and worked out in more detail in our earlier papers[24,25] for a polymer in a poor solvent. The essential idea is as follows: two flat parallel surfaces are immersed far apart in a polymer solution (polymer volume fraction ϕ_b) until polymer has adsorbed to an equilibrium adsorbance Γ. The monomer volume fraction $\phi(z)$ (at distance z from each surface) adopts a profile that minimizes the total (excess) Helmholtz free energy.

The surfaces are then brought together, subject to the constraint that the *surface excess* Γ *remains constant* (an assumption that is supported by experiments[19–23]); provided *local* equilibrium is maintained as the surface separation is varied, the monomer profile $\phi(z)$ adjusts itself to maintain the excess free energy at a minimum. In this way the equilibrium profile, the surface energy, and hence the disjoining pressure between the surfaces may be evaluated as functions of the distance between the polymer-bearing plates. Our calculations allow also for the washing away of polymer solution, and its replacement by pure solvent (subject always to a constant Γ), prior to changing the plate separation.

In this section we treat the adsorbed polymer structure at a single, flat surface. The Flory–Huggins theory for a polymer solution inscribed on a lattice (lattice constant a) can be expanded at low volume fraction ϕ to give the free-energy density

$$F(\phi) = (T/a^3)[(\phi/N)\ln\phi + (1/2)v\phi^2 + (1/6)w\phi^3 + ...] \quad \text{(II.1)}$$

where T is the absolute temperature in energy units (i.e., we work in units where Boltzmann's constant is unity), N is the degree of polymerization, v and w are proportional respectively to the second and third virial coefficients.[26] For a given polymer–solvent system there generally exists a temperature Θ for which v vanishes, while usually w is only weakly temperature-dependent and of order unity: e.g., $w \simeq 0.2$ for polystyrene in cyclohexane[11] and $w \simeq 0.75$ for poly(dimethylsiloxane) in bromocyclohexane.[11] Because the Θ temperature corresponds to a tricritical point, the mean-field Flory–Huggins theory should provide an adequate description (to within logarithmic corrections). Throughout this paper, we focus on Θ conditions; i.e., $v = 0$.

(a) Single Surface in Solution. For a single surface in equilibrium with polymer solution, the interfacial energy per unit area may be expressed as[6]

$$\gamma - \gamma_0 = \gamma_s(\phi_s^0) + \int_0^\infty [F(\phi) - \mu_b\phi + \pi_b + (T/24a\phi)(d\phi/dz)^2]\,dz \quad \text{(II.2)}$$

where γ_0 is the pure solvent interfacial energy density, $\mu_b \equiv (\partial F/\partial\phi)|\phi_b$ is the polymer chemical potential in the bulk, $\pi_b \equiv (\mu_b\phi_b - F(\phi_b))$ is the bulk osmotic pressure, z is the perpendicular distance from the wall, and the gradient term takes into account the free energy associated with concentration fluctuations that are slowly varying in space. The integrand in eq II.2 represents the *excess* free energy associated with creating, from a uniform bulk solution, unit volume of solution of concentration $\phi(z)$ at a distance z from the adsorbing surface. The function $\gamma_s(\phi_s^0)$ describes the local polymer–surface interaction in terms of ϕ_s^0, the surface polymer volume fraction. We expand γ_s in a power series

$$\gamma_s(\phi_s^0) = -\gamma_1\phi_s^0 + (1/2)\gamma_2(\phi_s^0)^2 + ... \quad \text{(II.3)}$$

where $\gamma_1 a^2$ is the "sticking" free energy per monomer and γ_2 relates to the surface-induced modification of the monomer–monomer interaction.[2] We retain only the first term in the expansion; the validity of this will be considered later in this section and in section VII.

It is convenient to transform the length scale to $x = z/\xi_b$, where $\xi_b = a/(w^{1/2}\phi_b)$ is the Edwards correlation length.[27] (Strictly, this interpretation of ξ_b is valid only under semidilute conditions, $\phi_b > \phi^* = N^{-1/2}$, but the scaling variable so-defined is useful over a wider range

of concentrations.) The polymer volume fraction is replaced by the reduced order parameter $y = (\phi/\phi_b)^{1/2}$. Combining eq II.1–II.3, we find (for $v = 0$, and dropping γ_2)

$$(\gamma - \gamma_0)/(\gamma_1\phi_b) = -y_s^2 + (\phi_b/\sigma)\int_0^\infty [y^6 + [\eta(\ln y^2 - 1) - 3]y^2 + (\eta + 2) + (dy/dx)^2]\, dx \quad \text{(II.4)}$$

where $y_s \equiv y(x = 0)$, and the surface coupling constant σ is

$$\sigma = (6\gamma_1 a^2/w^{1/2}T) \quad \text{(II.5)}$$

The parameter η, defined by

$$\eta = (\xi_b/R_g)^2 = (6/w)(\phi^*/\phi_b)^2 \quad \text{(II.6)}$$

(where $R_g = (N/6)^{1/2}a$ is the unperturbed radius of gyration of the polymer), gives the weight of the translational entropy of the polymer chains relative to the monomer–monomer repulsion in eq II.1 for $F(\phi)$ at the Θ point. For w of order unity and N typically $\sim 10^4$, η takes values from less than 1 at high incubation concentrations to $\sim 10^9$ for $\phi_b = 10^{-6}$. Thus, in the semidilute regime, where $\phi_b > \phi^*$, it is not unreasonable to neglect terms in η. This makes for simplification in the resulting algebra and allows us to extend significantly the analytical discussion of the model. In practice, however, because spontaneous adsorption of polymers takes place readily even from very dilute solutions, protective adsorption onto colloids is carried out mostly at low values of ϕ_b ($\phi_b \ll \phi^*$), where η is large. For this reason we shall generally include terms in η in our calculations; occasionally, where a particular insight emerges due to simplification of the analysis if η is neglected, we shall note explicitly the limiting behavior at high incubation concentration (i.e., $\phi_b > \phi^*$, η negligible).

The Euler–Lagrange equation to optimize eq II.4 with respect to $y(x)$ has a first integral

$$(dy/dx)^2 = y^6 + [\eta(\ln y^2 - 1) - 3]y^2 + \eta + 2 \quad \text{(II.7)}$$

where the constant of integration has been chosen so that the gradient vanishes in the bulk; i.e., $(dy/dx)|_{y=1} = 0$. Formal integration yields

$$x = \int_y^{y_s} [y^6 + [\eta(\ln y^2 - 1) - 3]y^2 + \eta + 2]^{-1/2}\, dy \quad \text{(II.8)}$$

which implicitly gives the concentration profile $\phi(z)$. For relatively strong adsorption, $\phi_s^0 \gg \phi_b$ or $y_s \gg 1$, the integrand is dominated by the first term, and the profile in the proximal region ($y \gg 1$) can be approximated by

$$\phi = \phi_s^0(1 + z/D)^{-1} \quad \text{(II.9)}$$

where the extrapolation length

$$D = (a/2w^{1/2}\phi_s^0) \quad \text{(II.10)}$$

is such that $D \ll \xi_b$. In the distal region ($y \simeq 1$) the profile approaches ϕ_b exponentially

$$(\phi - \phi_b/\phi_b) = 1 + A\exp[-(12 + 2\eta)^{1/2}z/\xi_b] \quad \text{(II.11)}$$

where A is a constant that depends on ϕ_b: it is of order unity for $\phi_b \geq \phi^*$, increasing approximately as $(\ln \eta)^2$ for lower incubation concentrations.

Inserting eq II.7 into eq II.4 and minimizing γ with respect to y_s yields the Cahn–de Gennes boundary condition

$$(dy/dx)|_{y_s} = (\sigma/\phi_b)y_s$$

or

$$(\sigma/\phi_b)^2 y_s^2 = y_s^6 + [\eta(\ln y_s^2 - 1) - 3]y_s^2 + \eta + 2 \quad \text{(II.12)}$$

For relatively strong adsorption we expect y_s [$\equiv(\phi_s^0/\phi_b)^{1/2}$] $\gg 1$, so that the right-hand side of eq II.12 is dominated by the first term, giving

$$y_s^2 \simeq (\sigma/\phi_b)$$

The corresponding surface volume fraction is then

$$\phi_s^0 \simeq \sigma \quad \text{(II.13)}$$

while a first-order correction (based on expanding eq II.13) gives

$$\phi_s^0 = \sigma + (3/\sigma wN)(1 - \ln(\sigma/\phi_b)) \quad \text{(II.13a)}$$

Substituting eq II.13 into eq II.10, we can check whether the assumption of strong adsorption ($D \ll R_g$) is consistent with the neglect of the γ_2 term in γ_s ($D \gg a$). These inequalities may be simultaneously satisfied, provided the monomer sticking energy $\gamma_1 a^2$ satisfies

$$N^{-1/2} \ll (\gamma_1 a^2/T) \ll 1 \quad \text{(II.14)}$$

A typical value of $(\gamma_1 a^2/T)$ is $\sim 10^{-1}$ and of $N^{-1/2}$, say, 10^{-2}, so the inequalities in eq II.14 can be obeyed simultaneously.

The incubation surface excess Γ_0, defined by

$$\Gamma_0 = a^{-1}\int_0^\infty (\phi - \phi_b)\, dz \quad \text{(II.15)}$$

becomes

$$\Gamma_0 = w^{-1/2}\int_1^{y_s} (y^2 - 1)[y^6 + [\eta(\ln y^2 - 1) - 3]y^2 + (\eta + 2)]^{-1/2}\, dy \quad \text{(II.16)}$$

In the low η limit ($\phi_b > \phi^*$), this expression simplifies to

$$\Gamma_0 = w^{-1/2}\int_1^{y_s} [y^2 + 2]^{-1/2}\, dy = (1/2w^{1/2}) \ln(\phi_s^0/\nu\phi_b) = (1/2w^{1/2}) \ln(\xi_b/2\nu D) \quad \text{(II.17)}$$

where $\nu = ((1 + \sqrt{3})/2)^2 \simeq 2$ is a constant. The result (eq II.17) deserves comment: it makes the seemingly strange prediction that the surface excess Γ_0 *decreases* with increasing incubation concentration ϕ_b. This is a consequence of the definition (eq II.15) of Γ_0, which is equivalent to the total volume of polymer segments away from an adsorbing surface *less* the total volume of polymer segments in the *bulk incubating solution* (both per unit area of surface). As the bulk concentration ϕ_b increases beyond ϕ^* (i.e., in the low η limit for which eq II.17 is valid), the polymer excess near the surface saturates and the *difference* given by Γ_0 decreases. In practice, measurements of adsorbance using conventional techniques (e.g., microbalance experiments) correspond to the definition (eq II.15) of Γ_0 only at the low ϕ_b limit (where eq II.17 is not valid), which is the usual situation in nearly all practical cases of interest. [Equation II.17 may be checked by measuring excess adsorbed polymer in an experiment where the effect of "background" polymer concentration (i.e., ϕ_b) is subtracted from the signal (for example, an evanescent wave probe extending beyond the cutoff $\phi = \phi_b$[14] or ellipsometric measurements[13])]. For this reason we shall mainly confine ourselves in this paper to discussion of the $\phi_b < \phi^*$ regime. In this regime it is found (see later) that there is an even weaker logarithmic dependence on ϕ_b, but now Γ_0 increases (as we would intuitively expect) as ϕ_b increases. There is a maximum

surface excess $\Gamma_0 = \Gamma_{max}$ near ϕ^*, given roughly by

$$\Gamma_{max} \simeq (1/2w^{1/2}) \ln (\phi_s^0/\nu\phi^*) \quad \text{(II.18)}$$

(b) Single Surface following Washing. If, following incubation as above, the polymer solution is replaced by pure solvent without any desorption of polymer (as frequently happens in real systems, where net sticking energies per molecule greatly exceed T), the profile $\phi(z)$ can be fixed by minimizing the augmented interfacial energy density

$$\hat{\gamma} = \gamma + \lambda\Gamma \quad \text{(II.19)}$$

where λ is a Lagrange multiplier chosen such that $\Gamma = \Gamma_0$. Due to the way in which Γ_0 has been defined in eq II.15, the expression eq II.19, and the subsequent development of this section, *is valid only in the dilute regime* $\phi_b < \phi^*$. In the Cahn–de Gennes formulation,[6] the excess free energy (eq II.2) is replaced by

$$\hat{\gamma} - \gamma_0 = -\gamma_1\phi_s + \int_0^\infty [F(\phi) - \hat{\mu}\phi + (T/24a\phi)(d\phi/dz)^2]\, dz \quad \text{(II.20)}$$

where $F(\phi)$ is still given by eq II.1 with $\upsilon = 0$, $\hat{\mu}$ (the pseudochemical potential) provides for irreversibility of the adsorption, the osmotic pressure term has disappeared because (following the washing) the bulk polymer concentration is vanishingly small, and ϕ_s is the surface volume fraction following the wash. As in the unwashed case, it is convenient to transform to dimensionless variables but now with ϕ_b replaced by ϕ^*, i.e., $x^* = z/\xi^*$ (where $\xi^* = a/(w^{1/2}\phi^*)$), and $y^* = (\phi/\phi^*)^{1/2}$. The interfacial energy becomes

$$[(\hat{\gamma} - \gamma_0)/(\gamma_1\phi^*) = -y^*_s{}^2 + (\phi^*/\sigma)\int_0^\infty y^{*6} + (\eta^* \ln y^{*2} + k)y^{*2} + (dy^*/dx^*)^2]\, dx^* \quad \text{(II.21)}$$

with $y^*_s = (\phi_s/\phi^*)^{1/2}$, $\eta^* = 6/w$, and k is a dimensionless Lagrange multiplier.

The first integral of the Euler–Lagrange equation for $y^*(x)$ is

$$(dy^*/dx^*)^2 = y^{*6} + (\eta^* \ln \gamma^{*2} + k)y^{*2} \quad \text{(II.22)}$$

and the surface volume fraction is fixed by

$$(\sigma/\phi^*)y^*_s{}^2 = y^*_s{}^6 + (\eta^* \ln y^*_s{}^2 + k)y^*_s{}^2 \quad \text{(II.23)}$$

The washed surface excess

$$\Gamma = a^{-1}\int_0^\infty \phi\, dz = w^{-1/2}\int_0^{y^*_s} y^*[y^{*4} + \eta^* \ln y^{*2} + k]^{-1/2}\, dy^* \quad \text{(II.24)}$$

is required to equal Γ_0. The washed profile is determined by solving eq II.23 and II.24 for y_s and k. Note that, in the region near the surface, the polymer volume fraction maintains the variation eq II.9 with ϕ_s^0 replaced by ϕ_s, while in the distal region the profile falls exponentially to zero.

III. Two Plate Interaction

In this section we evaluate the force between two surfaces onto which polymer has adsorbed to an adsorbance (or surface excess) Γ. Here Γ can take a maximal value Γ_0 corresponding to the equilibrium adsorption (with the two plates held far apart) from the original incubating solution at concentration ϕ_b (we limit ourselves in this section to the dilute regime $\phi < \phi^*$). However, it is also possible for Γ to be lower than Γ_0. This may arise in two ways:

(i) By holding the two surfaces close together during the incubation period, the rate of access of polymer to the gap between the plates can be diffusion limited. At short times, therefore, reproducible force profiles may be measured at adsorbance values lower than Γ_0. This procedure has been adopted in several of the experimental studies.[20b,22,23]

(ii) As noted in the Introduction, kinetic factors generally prevent desorption from a surface in the case where polymer has adsorbed to equilibrium ($\Gamma = \Gamma_0$) and the incubating solution has been subsequently washed. In a few cases (e.g., ref 23) some desorption has been noted when the incubating solution is massively diluted from ϕ_b to $\phi_{b'}$. In this case too, Γ can take values lower than Γ_0.

In all experiments to date, however, the value of Γ (whether equal to or lower than Γ_0) did not change on compression or decompression of the surfaces. With this in mind, we evaluate the interplate forces as a function of the separation $2h$ at bulk concentration $\phi_{b'}$, with the assumption of fixed Γ, and allowing also for $\phi_{b'}$ not necessarily equal to ϕ_b ($\phi_{b'} = 0$ corresponds to washed plates). As in the case of the washed single plate, the augmented interfacial energy $\hat{\gamma}$ of each plate is minimized subject to the constraint on Γ. Then the disjoining pressure (the force per unit area between the plates) is given by

$$\Pi = -(\partial\hat{\gamma}/\partial h) \quad \text{(III.1)}$$

The Cahn–de Gennes expression for $\hat{\gamma}$ based on eq II.2 and II.20 is

$$\hat{\gamma} - \gamma_0 = -\gamma_1\phi_s + \int_0^h [F(\phi) - \hat{\mu}\phi + \pi_{b'} + (T/24a\phi)(d\phi/dz)^2]\, dz \quad \text{(III.2)}$$

Performing the same scaling as for the single plate

$$(\hat{\gamma} - \gamma_0)/(\gamma_1\phi^*) = -y^*_s{}^2 + (\phi^*/a)\int_0^{h/\xi^*} [y^{*6} + (\eta^* \ln y^{*2} + k)y^{*2} + 2y^*_{b'}{}^6 + \eta^* y^*_{b'}{}^2 + (dy^*/dx^*)^2]\, dx^* \quad \text{(III.3)}$$

The first integral of the Euler–Lagrange equation for $y^*(x^*)$ is

$$(dy^*/dx^*)^2 = G(y^*) - G(y^*_m) \quad \text{(III.4)}$$

where

$$G(y^*) = y^{*6} + (\eta^* \ln y^{*2} + k)y^{*2} + 2y^*_{b'}{}^2 + \eta^* y^*_{b'}{}^6 \quad \text{(III.5)}$$

and the constant of integration is chosen for symmetry about the midplane, at which point $y^* = y^*_m$. The surface volume fraction satisfies the equation

$$(\sigma/\phi^*)^2 y^*_s{}^2 = G(y^*_s) - G(y^*_m) \quad \text{(III.6)}$$

The profile is fixed by two further equations:

$$h/\xi^* = \int_{y^*_m}^{y^*_s} [G(y^*) - G(y^*_m)]^{-1/2}\, dy^* \quad \text{(III.7)}$$

and

$$\Gamma = w^{-1/2}\int_{y^*_m}^{y^*_s} (y^{*2} - y^*_{b'}{}^2)[G(y^*) - G(y^*_m)]^{-1/2}\, dy^* \quad \text{(III.8)}$$

Simultaneous solution of eq III.6–III.8 for y^*_s, y^*_m, and k, combined with formal differentiation of eq III.2, leads to the disjoining pressure

$$\Pi = -(F - \mu\phi)|_b = -(wT/6a^3)(\phi^*)^3\, G(y^*_m) \quad \text{(III.9)}$$

We note that the bulk concentration after dilution $\phi_{b'}$ affects this solution only through the $y^*_{b'}{}^2$ term in eq III.8. This implies that for dilute bulk solution (the regime

$\phi_b < \phi^*$, $y^*_b < 1$, of interest in this section) there is little difference between the interaction of washed and unwashed interfaces. This is also consistent with the results of explicit calculations for the poor-solvent ($T < \theta$) case.[25]

At small separations ($h \lesssim D$) the profile is quite flat, and the solution to eq III.6–III.8 is readily found to be

$$\phi_m \simeq a\Gamma/h \qquad \text{(III.10)}$$

as $h \to 0$, the pressure tends to the limit

$$\Pi = (wT/3)(\Gamma/h)^3 \qquad \text{(III.11)}$$

This is consistent with de Gennes' predictions[6] and the poor-solvent results.[24,25] Notice that this repulsive behavior occurs for $h \lesssim D$, while the equilibrium position (eq III.11) varies, as a function of coverage, between $(2w^{1/2}\Gamma)^2 D$ and R_g. Thus we expect the low coverage minimum to be much sharper than that for saturated surfaces. Again this qualitative trend is consistent with experiment (see later).

IV. Computational Method

In order to obtain the interplate pressure, Π, it is necessary to solve eq III.6–III.8, given the surface excess Γ. In the case of saturation adsorption the surface excess must be calculated by finding ϕ_s^0 from eq II.13 then using this result to evaluate the integral (eq II.16); these are straightforward numerical procedures. Unsaturated interfaces (in the sense $\Gamma < \Gamma_0$) may be dealt with either (a) by treating them as saturated after incubation in polymer solution at some effective concentration ϕ_b less than the true concentration or (b) by simply choosing a value of $\Gamma < \Gamma_0$, e.g., assuming 10% coverage.

Since eq III.6 can be rearranged to express k explicitly in terms of y^*_s and y^*_m, the problem is reduced to the pair of simultaneous nonlinear equations

$$\tilde{A}(y^*_m, y^*_s) \equiv \int_y^{y^*_s} [G(y^*) - G(y^*_m)]^{-1/2}\, dy^* = h/\xi^*$$

and

$$\tilde{B}(y^*_m, y^*_s) \equiv \int_y^{y^*_s} y^{*2} [G(y^*) - G(y^*_m)]^{-1/2}\, dy^* = w^{1/2}\Gamma$$

Standard techniques may be employed to improve initial estimates of the limits of integration until a self-consistent solution is achieved. The pressure Π is then given by direct evaluation of eq III.9, and the interfacial energy density γ of each plate is calculated via step-by-step integration of Π from large separations $2h$ (where the interaction vanishes).

The computations are relatively rapid: for example, the time to calculate an interaction profile is around 60 s CPU time on an IBM 3081.

V. Computational Results

In this section we present selected results showing the major trends of behavior indicated by the numerical solutions of the relevant equations of our model (eq III.6–III.8), while varying the model parameters. Results for both the single plate and for interactions between two plates are shown.

To permit comparison with experimental results,[22,23] we have performed calculations with the parameters w, N, a, T, and σ chosen to describe polystyrene in cyclohexane (PS–CH) and polystyrene in cyclopentane (PS–CP) with mica plates. The third virial coefficient for PS–CH has been measured to be $w \simeq 0.2$;[11] that for PS–CP is not known so a range of w values between 0.2 and 1.4 was investigated. The degree of polymerization, N, and the lattice constant have somewhat ambiguous meanings for real polymers: N may be interpreted as the number of backbone units, monomers, or some longer effective group, and there are corresponding definitions of a. Here we assume that N is the number of styrene monomers in the macromolecule and a is then obtained via the relation $R_g^2 = Na^2/6$ where R_g, the radius of gyration in bulk solution, is a measurable quantity. (The literature values for R_g for polystyrene suggest that $a = 0.66 \pm 0.02$ nm.) The temperatures T chosen for the calculation were the Θ points for the two systems: 34.5 °C (PS–CH) and 19.6 °C (PS–CP).[23] Last, the surface coupling constant $\sigma = 6\gamma_1 a^2/w^{1/2}T$ contains γ_1, which cannot be determined directly, though it can be deduced from measurements of adsorbance or surface excess. The inequalities (eq II.14) restrict the possible range of σ, and for consistency with the poor-solvent case[24,25] even tighter limits must be imposed: for PS–CH, $0.2 < \sigma < 1.0$ approximately, so the value $\sigma = 0.6$ has been taken as standard.[28]

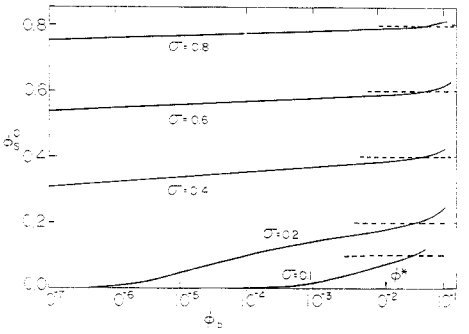

Figure 1. Variation of the surface volume fraction ϕ_s^0 with incubation concentration ϕ_b, for $w = 0.2$, $N = 6000$, and different values of the surface coupling constant σ: (a) $\sigma = 0.8$; (b) 0.6; (c) 0.4; (d) 0.2; (e) 0.1. The broken lines show the value $\phi_s^0 = \sigma$ for the respective curves.

(a) Single Plate. Figure 1 shows the variation of the surface volume fraction ϕ_s^0 with incubation concentration ϕ_b. For ϕ_b in the semidilute regime ($\phi_b > \phi^*$), $\phi_s^0 \sim \sigma$, in accordance with eq II.13. As ϕ_b is decreased in the dilute regime ($\phi_b < \phi^*$), there is a smooth falloff in ϕ_s^0. For $\sigma \geq 0.4$, the weak logarithmic increase of ϕ_s^0 with ϕ_b is in good agreement with eq II.13a over the whole range of ϕ_b, indicating strong adsorption. In the case of the lower values of the surface coupling constant, $\sigma = 0.1$ and 0.2, the falloff with ϕ_b is more rapid. This suggests that these cannot be examples of strong coupling (in the sense discussed in section II).

Figures 2 and 3 show the segment concentration profile $\phi(z)$ for the single plate. Figure 2 shows the effect of different molecular weights on the profile, keeping the other parameters constant. As expected, the longer adsorbed chains extend further into solution. The inset shows the same data when the spatial axis z is scaled as z/ξ^*: since $\xi^* = (6/w)^{1/2}R_g$, this is equivalent to scaling the z-axis by the radius of gyration; the resulting close correspondence of the profiles (inset, Figure 2) emphasizes a universal profile at $z \gtrsim R_g/2$.

Figure 3 shows the variation of $\phi(z)$ with different incubation concentrations, from very dilute to well into the semidilute regime. Recalling (Figure 1) that the surface volume fraction ϕ_s^0 is practically constant in this concentration regime, these results (Figure 3) show that the proximal profile ($z \leq D$, where $D = (a/2w^{1/2}\varphi_s^0)$) is almost independent of φ_b for a given σ. This is consistent with eq II.9 for the strong adsorption case. Changing σ, on

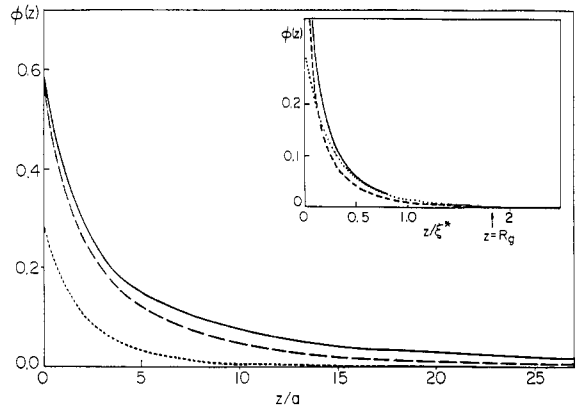

Figure 2. Segment concentration profile $\phi(z)$ as a function of distance z from the adsorbing plate, for $w = 0.2$, $\sigma = 0.6$, $\phi_b = 1.5 \times 10^{-5}$, and three different values of N: (···) $N = 1000$; (- - -) $N = 6000$; (—) $N = 20\,000$. The inset shows $\phi(z)$ with the z-axis normalized by the correlation length ξ^* ($\equiv(6/w)^{1/2}R_g$).

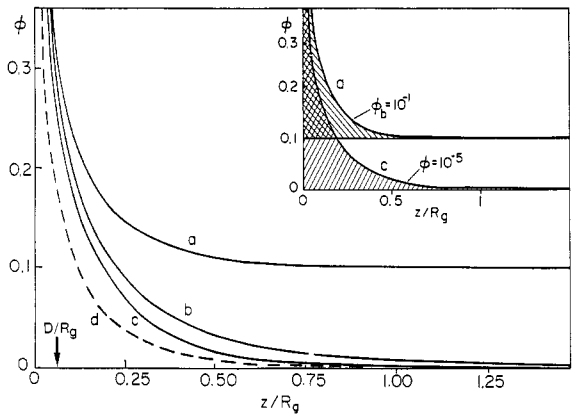

Figure 3. Segment concentration profile $\phi(z)$ for $N = 6000$, $w = 0.2$, $\sigma = 0.6$, and various incubation concentrations: (a) $\phi_b = 0.1$; (b) $\phi_b = 10^{-3}$; (c) $\phi_b = 10^{-5}$. The broken curve (d) shows the effect for $\phi_b = 10^{-5}$ [curve (c)] of increasing the third virial coefficient to $w = 1.0$. The shaded areas in the inset correspond to the surface excess Γ_0 for curves (a) and (c) and illustrate how Γ^0 (defined in eq II.6) can actually drop with increasing ϕ_b for $\phi_b > \phi^*$. (See also text following eq II.17.)

the other hand (for fixed w, ϕ_b), has little effect on $\phi(z)$ for $z \geq D$ (not plotted). Also shown (broken curve) is the effect of increasing the value of the third virial coefficient w. In general, such an increase corresponds to a higher (repulsive) osmotic interaction for any given $\phi(z)$ and to a lower surface excess Γ_0 (see also Figures 4 and 5) for a given surface coupling σ. The inset to Figure 3 shows more directly how the surface excess Γ_0 defined in eq II.16 is extracted from the $\phi(z)$ profiles. In particular, it illustrates clearly how Γ_0 (the shaded area in the inset) actually drops with increasing ϕ_b at $\phi_b > \phi^*$, as discussed at length following eq II.17. We note that in the proximal region of the profiles in Figures 2 and 3 the volume fraction does not satisy $\phi \ll 1$ nor is the rate of spatial variation $(1/\phi)|(d\phi/dz)|$ small. These deviations from the assumptions that went into the derivation of eq II.4 will be discussed in section VII.

Figures 4 and 5 show how Γ_0 varies with the bulk incubation concentration ϕ_b. All curves increase approximately logarithmically with ϕ_b to a maximum in Γ_0 just below ϕ^*; for $\phi > \phi^*$, the surface excess falls in accord with eq II.18, with a stronger logarithmic slope. Figure 4 shows that, under otherwise identical conditions, longer chains tend to higher adsorbance of polymer than those with low N. This is qualitatively reasonable for strong surface coupling. The effect of increasing w is also shown

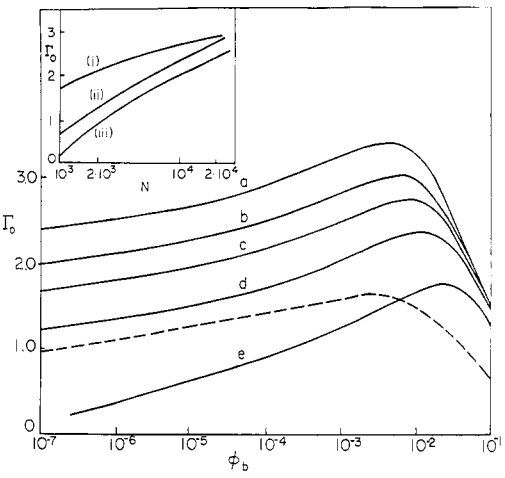

Figure 4. Variation of the polymer surface excess Γ_0 with incubation volume fraction ϕ_b for $w = 0.2$, $\sigma = 0.6$, and various values of N: (a) $N = 20\,000$; (b) 10 000; (c) 6000; (d) 3000; (e) 1000. The broken curve shows the effect for $N = 6000$ [curve (c)] of increasing the third virial coefficient to $w = 1.0$. The inset shows the variation of Γ_0 with N, for three different incubation concentrations: (i) $\phi_b = 0.02$, (ii) $\phi_b = 1.5 \times 10^{-5}$, (iii) $\phi_b = 10^{-7}$.

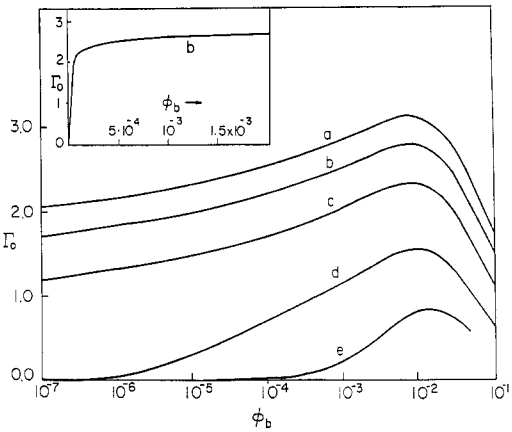

Figure 5. Variation of the polymer surface excess Γ_0 with incubation volume fraction ϕ_b for $N = 6000$, $w = 0.2$, and different values of the surface coupling constant σ: (a) $\sigma = 0.8$; (b) 0.6; (c) 0.4; (d) 0.2; (e) 0.1. The inset shows curve (b) on a linear–linear plot for $\phi_b < \phi^*$, showing the characteristic plateau behavior.

for fixed N and σ (broken curve): the resulting decrease in Γ_0 is in accord with the idea that the increase in osmotic repulsion resulting from the higher third virial coefficient reduces the number of adsorbed chains. The inset to Figure 4 shows that Γ_0 varies approximately logarithmically with N, over the range of N studied, for two dilute incubation concentrations ($\phi_b \ll \phi^*$), curves (ii) and (iii) in the inset. For $\phi_b \geq \phi^*$ (curve (i) of the inset) the behavior is more complicated, though in general the dependence of Γ_0 on N in this regime is much weaker. Indeed, for the case where the incubating solution is at $\phi_b \gg \phi^*$, a plateau is indicated for Γ, as shown for $\phi_b = 0.02$ (curve (i), inset). At this value of the incubation concentration ϕ^* is initially ($N = 1000$, $\phi^* = 0.032$) greater than ϕ_b but eventually (for $N > 2500$) falls below it. This plateau-like behavior has indeed been observed for adsorption from Θ solvents.[12]

Figure 5 illustrates the effect of surface coupling σ on the adsorbance: once again, as intuitively expected, stronger surface coupling corresponds to higher adsorbed amount (in the strong adsorption regime), while the qualitative differences between $\sigma \gtrsim 0.2$ and $\sigma < 0.2$ (i.e., strong vs weak adsorption) are evident. The inset shows data

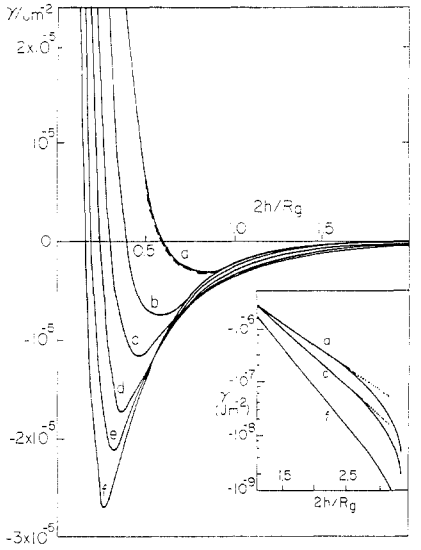

Figure 6. Interaction energy γ per unit area (per plate), for plates with adsorbed polymer, as a function of scaled plate separation $2h/R_g$. Curves are plotted for $N = 6000$, $w = 0.2$, $\sigma = 0.6$, and various incubation concentrations ϕ_b in the dilute regime ($\phi_b < \phi^*$): (a) $\phi_b = 10^{-3}$; (b) 10^{-4}; (c) 1.5×10^{-5}; (d) 10^{-6}; (e) 10^{-7}; (f) 10^{-8}. The broken curve shows the (small) effect of replacing the solution by pure solvent for the case $\phi_b = 10^{-3}$ [curve (a)]. The inset shows the attractive tail of the interaction profile for three of the incubation concentrations, indicating a quasi-exponential decay.

for one of the curves on a linear–linear plot, reproducing the classical "plateau" behavior.[13,29]

We observe that the surface excess Γ_0 data of Figures 4 and 5 are rather well described for dilute incubation concentrations $\phi_b \lesssim 0.1\phi^*$ (the usual range of practical interest) by the relation

$$\Gamma_0 = (1/4)w^{-1/2} \ln [R_g^2/(D^2 \ln (c\phi_s^0/\phi_b))] \quad \text{(V.1)}$$

where $c = 0.03$ is chosen to obtain the best fit. This relation is obtained from eq II.16 by approximating $\{[\eta(\ln y^2 - 1) - 3]y^2 + \eta + 2\}$ by $\eta y^2 \ln (cy_s^2)$. The agreement between eq V.1 and the full (numerical) solution to eq II.16 in Figures 4 and 5 is better than 5% over the whole $\phi_b \lesssim 0.1\phi^*$ range; (the fit is poorer for $N \lesssim 3000$ in Figure 4 and for $\sigma \lesssim 0.4$ in Figure 5).

(b) Interactions between Two Surfaces. Unless otherwise stated the results in this subsection are for unwashed plates (using eq III.5a and III.8a) following (quasi-irreversible) adsorption to saturation; the same bulk concentration is assumed throughout incubation and interaction between the plates. As noted following eq III.8a, washing makes very little difference to the interaction profiles at $\phi_b < \phi^*$; this will be demonstrated by an explicit example below.

In Figures 6–9 interfacial free-energy densities $\gamma(h)$ are plotted as a function of plate separation $2h$ (scaled by R_g). [As will be explained in the next section, the interfacial energy (i.e., the interaction energy per unit area per plate) for flat parallel plates can be directly related to the forces measured between two curved surfaces with adsorbed polymer.] All the curves have three main qualitative features in common: a strong repulsive wall for small separations; the existence of an equilibrium separation $2h_{eq}$, where $\Pi = 0$ and $\gamma = \gamma_{min}$; and an attractive tail with an approximately exponential decay as $h \to \infty$.

Figure 6 shows the effect of changing the incubation concentration in the dilute regime $\phi_b < \phi^*$. As ϕ_b increases, it is found that the spatial scale expands: e.g., $h_{eq} = 0.13R_g$ for $\phi_b = 10^{-8}$, but $h_{eq} = 0.27R_g$ at $\phi_b = 10^{-4}$. This is to be expected, since it is assumed that all interaction between the plates is induced by layer overlap or bridging (the range of which increases with adsorbed layer thickness); the effective thickness of the adsorbed layer on each plate increases with ϕ_b. We shall see that, for a given w, a similar effect is observed whenever the adsorbed layer becomes thicker, whether due to changes in ϕ_b, σ, or N.

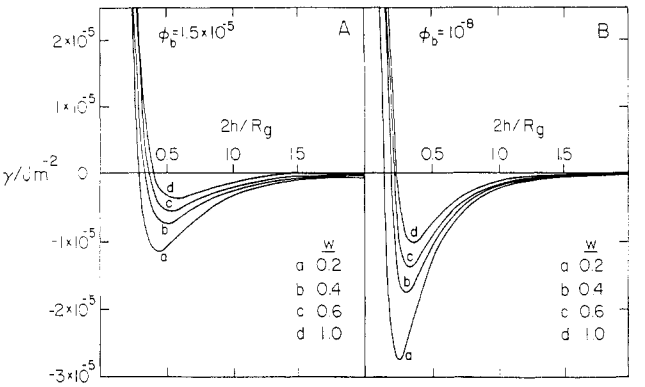

Figure 7. Interaction profiles γ vs $(2h/R_g)$ for $N = 6000$, $\sigma = 0.6$, and different values of the third virial coefficient w: (a) $w = 0.2$; (b) $w = 0.4$; (c) $w = 0.6$; (d) $w = 1.0$. Parts A and B of Figure 7 show the behavior at two different incubation concentrations, $\phi_b = 1.5 \times 10^{-5}$ and 10^{-8}, respectively.

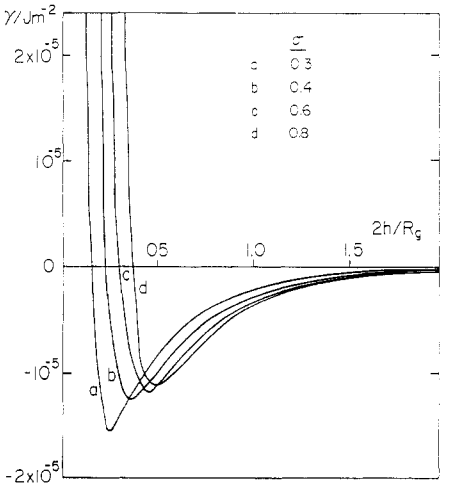

Figure 8. Interaction profiles γ vs $(2h/R_g)$ for $N = 6000$, $w = 0.2$, $\phi_b = 1.5 \times 10^{-5}$, for different values of the surface coupling constant σ: (a) $\sigma = 0.3$; (b) 0.4; (c) 0.6; (d) 0.8.

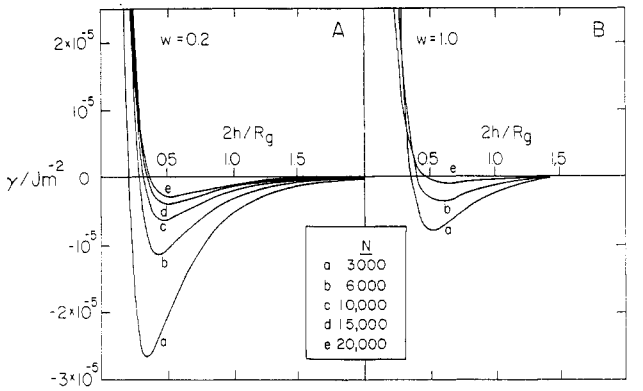

Figure 9. Interaction profiles γ vs $(2h/R_g)$ as a function of degree of polymerization, N, for $\sigma = 0.6$, and $\phi_b = 1.5 \times 10^{-5}$: (a) $N = 3000$; (b) $N = 6000$; (c) $N = 10\,000$, (d) $N = 15\,000$; (e) $N = 20\,000$. Figure 9A is for $w = 0.2$, while Figure 9B shows three of the profiles for $w = 1.0$.

Also, as ϕ_b increases, γ_{min} becomes less negative; i.e., the maximum strength of the attraction between the plates lessens. This results from a shift in the balance between competing effects:

(i) The surface volume fraction ϕ_s increases with ϕ_b, so the total surface sticking energy increases. This helps to make λ_{min} more negative.

(ii) The surface excess increases with ϕ_b. This increases monomer–monomer repulsion throughout the profile, tending to countereffect (i).

(iii) Bridging of the gap by a single polymer molecule, which always leads to attraction, is inhibited by increasing the surface excess.

Contribution (ii) is of second-order at the Θ point, and in any case a similar trend is found for poor solvents,[24,25] where the monomer–monomer interaction is attractive. Therefore, it seems likely that bridging makes the dominant contribution toward determining this behavior.

The exponential nature of the attractive tail is shown in the inset.

Also shown in Figure 6 is the *washed* $\gamma(h)$ profile (broken curve) for $\phi_b = 10^{-3}$: the highest incubation concentration shown in Figure 6, for which the effect of washing would be expected to be greatest. The difference between washed and unwashed profiles is negligible. As discussed in section III, this is a general feature for all $\phi < \phi^*$. (Recall that $\phi^* \simeq 10^{-2}$ for $N = 6000$.)

The effect of changing the third virial coefficient w is shown in parts A and B of Figure 7 for two different values of the incubation concentration ϕ_b. The general trend is that smaller w values, associated with greater surface excesses (see Figure 4), show stronger atraction. This runs counter to the trend indicated in Figure 6, where it was the *lower* surface excess values that resulted in the stronger attraction. We deduce that the repulsive osmotic contribution at the higher w values more than compensates for the increased bridging attraction that results from the lower Γ_0 at those w values. For any *given* w, however, the attraction is much stronger at a lower adsorbance (resulting from a lower ϕ_b), as can be seen by comparing parts A and B of Figure 7 for which $\phi_b = 10^{-5}$ and 10^{-8}, respectively.

When the surface coupling parameter σ is increased, the surface excess rises and there is a trend toward longer ranged, but weaker, interactions, as shown in Figure 8. This is in accord with the trend noted earlier for higher Γ_0 resulting from higher ϕ_b (Figure 6). However, for a comparable increase in Γ_0, the effect on the interaction profile is much smaller at fixed ϕ_b, w (Figure 8) than at fixed σ, w (Figure 6). The reason is that an increased σ promotes stronger bridging attraction, which partially negates the greater osmotic repulsion resulting from higher Γ_0 values.

In parts A and B of Figure 9 the molecular weight is varied for two values of the third virial coefficient w. The trend with increasing N (and thus Γ_0) is toward a longer ranged but weaker interaction, which is consistent with an increased effective polymer layer thickness; this, for a given plate separation, results in increased osmotic repulsions and reduced bridging. For the higher N values, the interaction profile at $w = 1.0$ (Figure 9B) looks almost monotonically repulsive on the scale drawn: this will be referred to again in the next section where comparison is made with experimental results. Perhaps surprisingly, the range of interaction, as measured by h_{eq} or the position of the repulsive wall, does not scale as $R_g \sim N^{1/2}$ but moves out more rapidly as N increases at the lowest N values. There is, however, a trend toward a limit $h_{eq} \simeq 0.3R_g$ (Figure 9A).

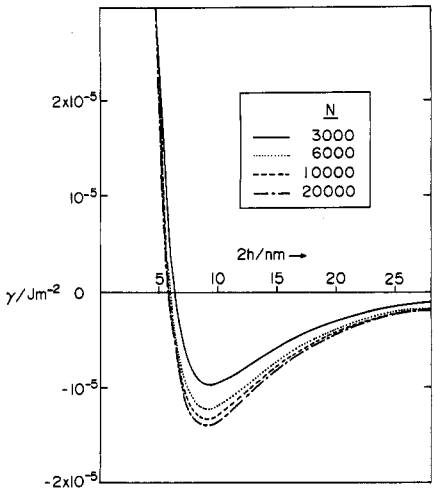

Figure 10. Interaction profiles γ vs $2h$ of washed plates as a function of degree of polymerization, N, for $w = 0.2$, $\sigma = 0.6$, and $\Gamma = 2.0$. Note that the *adsorbance*, rather than the bulk incubation concentration, is the same in each case.

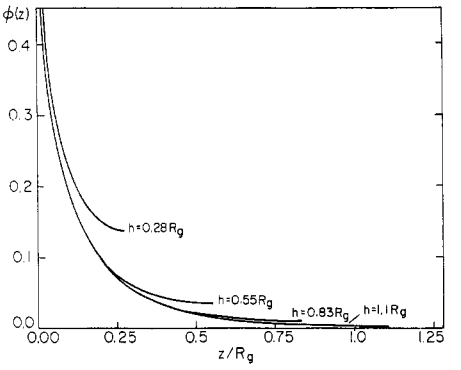

Figure 11. Segmental density distribution $\phi(z)$ between two polymer-bearing surfaces as a function of distance z from one of the surfaces, shown for various interplate half-separations h. $N = 6000$, $w = 0.2$, $\sigma = 0.6$, $\phi_b = 1.5 \times 10^{-5}$. (The distribution is symmetric about $z = h$; only one half of the distribution is shown.)

The trend with increasing N is almost entirely due to the change in the amount of polymer that adsorbs from a solution having a given monomer volume fraction ϕ_b. This may be demonstrated, as in Figure 10, by fixing the *surface excess* Γ, rather than ϕ_b, to be the same for each N. The resulting profiles (Figure 10) show that both the range (note that the spatial axis is *not* scaled by R_g) and strength of the intreaction are almost independent of N.

The final profile selected from our results shows the segmental density distribution between the two plates as they are brought together. The profiles in Figure 11 (which are qualitatively similar to those for other ϕ_b and w values) show that the polymer volume fraction falls in a smooth, monotonic fashion, as one moves away from the plates, without exhibiting the points of inflection which have been calculated for the poor-solvent case.[24,25] For separations $2h \gtrsim R_g$, there is little modification of the profile in the proximal region (say, within $z \simeq 0.25R_g$ of the walls). In the initial stages, the principal effect of bringing the surfaces together is to compress the polymer tail into the central part of the interplate gap ($z \gtrsim 0.25R_g$ from each wall). This reduces the free energy associated with slow spatial variations in concentration and increases the contribution of bridging. Both effects result in an attractive contribution to the net force, which, as

seen in all our interaction profiles, initially outweighs the increase in osmotic repulsion.

Overall, our results show a great richness of behavior, with the trends depending in detail on the variation of the different parameters. In the next section we compare the results of our model with available experimental data, especially that involving the force measurement technique for determining $\gamma(h)$.

VI. Comparison with Experiment

Several studies over the past two decades have investigated adsorption of polymer from Θ solvent onto solid surfaces. A comprehensive recent study is that by Takahashi et al.[12] There have been far fewer studies of interaction between two plates in polymer solutions; the most direct of these, for polymer in near-Θ solvents, have been the studies by Almog and Klein[23] on polystyrene in cyclopentane (PS–CP) and by Israelachvili et al.[22] on polystyrene in cyclohexane (PS–CH). In both cases the mica technique[17-19] was used: this measures the forces $F(D)$ between two curved mica surfaces in polymer solution as a function of the distance D between them. When the mean radius of curvature R of the surfaces is measured, it is possible, with use of the Derjaguin approximation,[19] to recast the results as

$$F(D)/2\pi R = 2\gamma(D) \qquad \text{(VI.1)}$$

where $\gamma(D)$ is the interaction energy per unit area (per plate) of flat parallel plates interacting with the same force law. This is identical with the definition of γ in our calculations and enables us to make direct comparison between the predictions of our model and the experimental data.

(a) Polystyrene–Cyclohexane–Mica.[22] In this system experiments were carried out both below the Θ temperature, at 24 °C (Θ = 34 °C), and slightly above it, at 37 °C (Θ + 3 °C). At each temperature, measurements were made on two PS samples, with molecular weights $M = 6 \times 10^5$ (PS1) and $M = 9 \times 10^5$ (PS2).

A remarkable feature of this study was that, as the temperature was raised from $T < \Theta$ to slightly above Θ, the attractive well noted at $T < \Theta$ did not disappear but was quite marked also at the higher temperature, where segment–segment interactions should no longer have been attractive. There was evidence for some desorption of polymer as the temperature was raised; the suggestion was put forward at the time that such desorption might have led to enhanced *bridging*, which was responsible for the persistence of attraction at the higher temperature. We can compare these experimental features with our calculated results both for the earlier $T < \Theta$ model[24,25] and from the present $T = \Theta$ calculations.

For PS1 ($M = 6 \times 10^5$, corresponding to $N = 6 \times 10^3$), the calculated surface excess[32] for $\phi_b = 11 \times 10^{-6}$, $w = 0.2$ at 24 °C was $\Gamma_0 = 4.2$, while for $T = \Theta = 34$ °C, $\phi_b = 11 \times 10^{-6}$, $N = 6 \times 10^3$, $w = 0.2$, and $\sigma = 0.6$[28] we find (Figure 4 in the current paper) $\Gamma_0 = 2.0$; i.e., the calculations predict that about half the adsorbed PS1 desorbs on heating from 24 to 34 °C.[32] This is consistent with the observed desorption noted in ref 22, Figure 5, where the "hard-core" repulsion at very strong compressions—which we may take as being due to essentially bulk polymer—is reduced in range by a factor of 2 when the temperature is raised from 24 to 37 °C ($T = \Theta - 10$ °C to Θ + 3 °C).

The calculated interaction profiles corresponding to the experiments of ref 22 are shown in Figure 12a for PS1 ($N = 6000$, $R_g = 21$ nm) at both $T = 24$ °C (from the earlier calculations of ref 25) and $T = \Theta = 34$ °C (from the present calculations). The values of the parameters used in the Θ case are $w = 0.2$, $\sigma = 0.6$, and $\phi_b = 10^{-5}$, which we estimate as being close to the corresponding experimental parameters.[28]

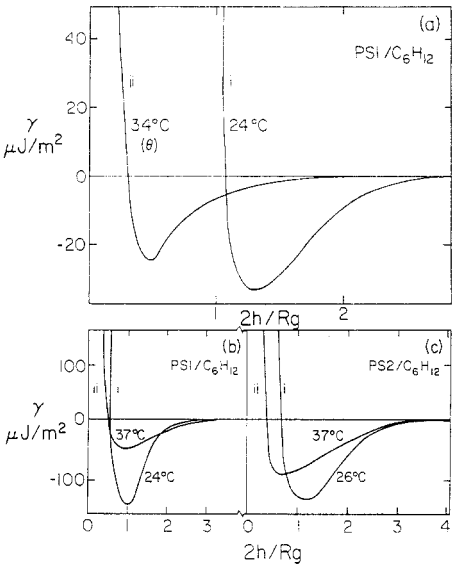

Figure 12. (a) Calculated interaction profiles between surfaces bearing adsorbed polystyrene, PS1 ($M = 6 \times 10^5$) in cyclohexane at 24 °C (curve (i), taken from ref 25) and at the Θ temperature 34 °C (curve (ii), this study). The parameters used are $N = 6000$, $w = 0.2$, $\sigma = 0.6$, and $\phi_b = 1.1 \times 10^{-5}$ chosen to correspond to the actual experimental conditions.[19,22,25] (b) Experimentally measured interactions between mica surfaces bearing PS1 at 24 °C [curve (i)] and at 37 °C [curve (ii)], following adsorption from PS1–cyclohexane solution ($\phi_b = 1.1 \times 10^{-5}$), taken from ref 22. (c) As in (b) but for PS2 ($M = 9 \times 10^5$): curve (i), 26 °C; curve (ii), 37 °C.

We observe (Figure 12a) that heating the system from $T = \Theta - 10$ °C to $T = \Theta + 3$ °C does not eliminate the attractive interaction, though it does reduce its magnitude somewhat. Thus, $2|\gamma_{min}|(T = \Theta - 10$ °C) = 31 μJ m^{-2}, while $2|\gamma_{min}|(T = \Theta) = 25$ μJ m^{-2}. The residual attraction is due to bridging, as discussed earlier. At the same time, the spatial scale of the interactions is compressed, so that the interaction minima are at $1.25R_g$ and $0.5R_g$, for $T = \Theta - 10$ °C and $T = \Theta$, respectively. Qualitatively, this is because the attractive interaction for $T < \Theta$ occurs when opposing *segments* overlap, while for $T = \Theta$ the bridging takes place when segments from one layer reach the other *surface*, i.e., at about half the range, as indeed shown by the calculations.

The experimental data for PS1 and PS2 are shown in parts b and c of Figure 12.[30] The main observed features are qualitatively in good accord with the calculated ones: a lower residual attraction as T increases from $T < \Theta$ to $T = \Theta$ and a contraction of the spatial scales. However, the absolute magnitude of the observed $|2\gamma_{min}|$ at $T = \Theta + 3$ °C is about a factor of 2–3.5 bigger than the calculated $|2\gamma_{min}|$ for $T = \Theta$. The reduction in the spatial scales, on heating from below to just above Θ, while certainly marked (especially for PS2, Figure 12c), is appreciably less than the calculations would indicate. This quantitative discrepancy (which may be in part due to the experiments having been done a little above Θ while the calculations are for $T = \Theta$) will be discussed in the last section; we note, however, the remarkable similarity of the main features between calculated (Figure 12a) and observed[22] profiles (Figure 12b,c) as the temperature is raised from below to just above Θ.

(b) Polystyrene–Cyclopentane–Mica (PS–CP). The Θ temperature for this system is 19.6 °C, and experi-

Table I
Values of Relative Adsorbed Amounts of PS on Mica from Cyclopentane, Estimated According to the Procedure in the Appendix[a]

item	data	sample	h_c, nm	m,[b] mg m^{-2}
a	Figure 3	PS1	19 ● 2	2.5 ● 1.5

item	data	sample	h_c, nm	Γ/Γ_o	m,[c] mg m^{-2}
b	Figure 4	PS5	6 ± 1	0.36	1.2
c	Figure 5a	PS5	12 ± 1	0.56	1.8
d	Figure 5b	PS5	19 ± 2	0.76	2.5
e	Figure 5c	PS5	29 ± 2	1.0	3.3

[a] The experimental force profiles are from figures in ref 23; the relative Γ values are based on h_c values estimated from a γ_c corresponding to $F/R = 10^3$ μN m^{-1} in all cases. [b] From refractive index data.[23] [c] By comparison with m(PS1). Relative error as for m(PS1). Items b–e were used to generate the theoretical profiles of Figure 14.

ments were carried out[23,34] at 23 ± 1 °C, i.e., at Θ + 3 °C, similar to the PS–cyclohexane case of the previous subsection. Polystyrene of two molecular weights was studied, PS1 as before ($M = 6 \times 10^5$) and PS5 ($M = 2 \times 10^6$). The main features to emerge from the study by Almog and Klein[23] were as follows:

(a) At low adsorbance of polymer (achieved by diffusion limiting the rate of adsorption), a marked attractive well is noted.

(b) As more polymer adsorbs (i.e., increasing surface excess), the attractive well diminishes, until at the limiting adsorbance (from a solution of $\phi_b = 1.5 \times 10^{-5}$) there is little detectable attraction: i.e., the force–distance profile appears (within the scatter) to be monotonically repulsive.

(c) On dilution of the PS–CP solution (after limiting adsorbance was reached) by about 10^4-fold and equilibration at the new bulk volume fraction ($\phi_b \sim 10^{-9}$), some polymer desorbs, and an attractive well is once again measureable. In what follows we compare our calculated predictions with these observations. We use N values of 6×10^3 and 2×10^4 for PS1 and PS5, corresponding to $M = 6 \times 10^5$ and $M = 2 \times 10^6$, respectively.

For a convincing comparison of calculated with observed data, it is necessary to have a measure of the adsorbance corresponding to each interaction profile. This data is not available for every profile in this study, but we may make an estimate of the relative adsorbed amounts from the observed repulsion at high compressions: we choose a particular value of the interaction energy, say, γ_c. Then the surface separation $2h_c$ at which $\gamma(h_c) = \gamma_c$ leads to a rough estimate of the corresponding adsorbed amount as $\Gamma \propto (h_c)^{2/3}$ (see Appendix). The values thus deduced are given in Table I.

We also require a value for the third virial coefficient for the PS–CP system, which (unlike w for the PS–cyclohexane system) has not been directly measured. The trend indicated for the PS–CP study, in particular the absence of bridging interaction for equilibrium adsorption from a $\phi_b = 1.5 \times 10^{-5}$ solution, suggests (see Figure 7A) that a relatively high value of w applies in this case. Thus the adsorbance values of PS1–cyclohexane at $T = \Theta + 3$ °C (Figure 12b) and for PS1–cyclopentane at $T = \Theta + 3$ °C (ref 23) (both at $\phi_b \sim 10^{-5}$) are similar (2–3 mg m^{-2}). However, the residual attraction in the former case (for which $w = 0.2$[25]) is much more marked than that in the latter, suggesting a value of w for the PS–CP system considerably greater than 0.2. (cf. Figure 7A). We therefore take $w = 1$ as standard for this system; we have also carried out calculations for $w = 0.6$, which give rather similar results.

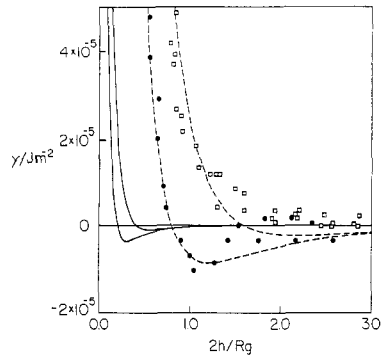

Figure 13. Calculated (solid lines) and experimental (ref 23) interaction profiles for PS5 ($M = 2 \times 10^6$) in cyclopentane at Θ + 3 °C and at $\phi_b = 1.5 \times 10^{-5}$ (□, ref 23, Figure 6) and following a ca. 10^4-fold dilution (●, ref 23, Figure 7). The broken curves are based on the calculated solid lines, with the interaction strength multiplied by a factor $\alpha = 2.4$ and the surface separation by a factor $\beta = 3.8$.

Having chosen w, we may now estimate the surface coupling constant σ for the PS–CP system, proceeding as follows: in the PS–CP experiments[23] the polymer solution (for PS5 at $\phi_b = 1.5 \times 10^{-5}$) was replaced by pure cyclopentane, resulting in a 10^4-fold dilution. This led to a desorption of polystyrene. These data are reproduced in Figure 13. From Figure 13 we estimate (see Appendix) that reducing ϕ_b from 1.5×10^{-5} to $\sim 10^{-9}$ reduces Γ by 20%. For $w = 1.0$, the value of σ that leads to a 20% fall in Γ, as calculated from eq II.17, corresponding to such a reduction in ϕ_b, is $\sigma = 0.27$. In subsequent comparisons of theory with experiment, therefore, we shall take $w = 1$ and $\sigma = 0.27$.

Also shown in Figure 13 (solid curves) are the calculated profiles for $\phi_b = 1.5 \times 10^{-5}$ and 10^{-9} for these values of w and σ. While it is clear that both the spatial extent and the energy scales are considerably compressed relative to experiment (we shall refer to this point in the following section), we note that the main qualitative features of the experiment are well accounted for. We have highlighted this by scaling the calculated values in both axes in order to best superpose them on the data. To do this, we have multiplied the force axis by a factor $\alpha = 2.4$ and the separation axis by a factor $\beta = 3.8$. The resulting curves are shown as broken lines in Figure 13.

Figure 14 shows the experimental force profiles between adsorbed PS5 layers at increasing Γ values (taken from ref 23). We have estimated the relative surface excess values in the manner described in the Appendix (see also Table I) and used them to calculate the corresponding force profiles. We then applied the identical scaling procedure as for Figure 13 to generate the broken curves superposed on the data. We note especially the rather good qualitative prediction of the trends of the data; however, our scaling procedure implies that, as in Figure 13, the calculated values of the energies and separation are too low by factors α and β, respectively.

Finally, Figure 15 shows the interaction profiles for PS1 and PS5 at $\phi_b = 1.5 \times 10^{-5}$ following limiting adsorption ($\Gamma = \Gamma_0$). The separation scales are normalized with respect to the radii of gyration. Using the standard w and σ values as before, we have calculated the corresponding force profiles. These have been scaled (by factors α and β), as in Figures 13 and 14, and are shown as broken curves superposed on the data. We note the rather good qualitative fit, especially in the high-repulsion regime. In particular, we note that scaling the calculated PS1 profile using the same multiplicative factors α and β results

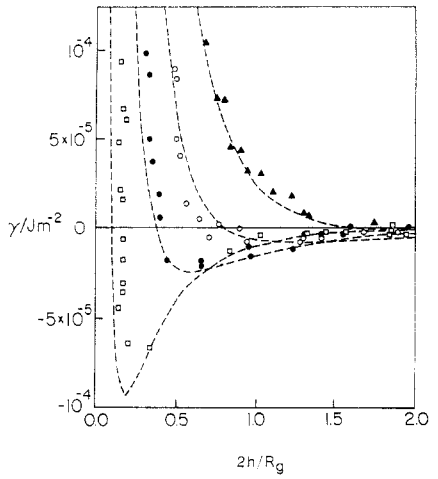

Figure 14. Measured force–distance profiles between mica surfaces bearing adsorbed PS5 layers in cyclopentane at $T = \Theta + 3$ °C (ref 23, Figure 5), at increasing Γ values (Γ increases from left to right, with the symbols farthest to the right corresponding to equilibrium adsorbance at $\phi_b = 1.5 \times 10^{-5}$). The broken curves are the corresponding calculated values, for $T = \Theta$, $w = 1.0$, and $\sigma = 0.27$, multiplied by the same factors α and β as in Figure 13 along the force and surface-separation axes, respectively.

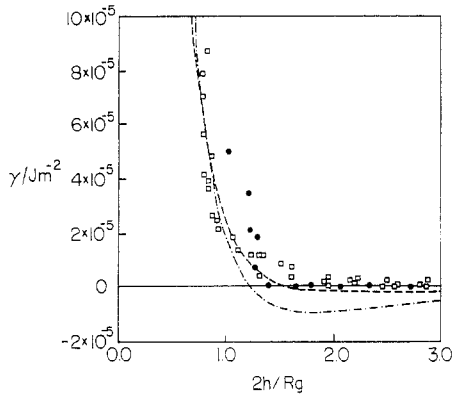

Figure 15. Measured interaction profiles between mica surfaces bearing adsorbed PS1 (●, ref 23, Figure 6) and PS5 (□, ref 23, Figure 6) in cyclopentane at 23 °C ($T = \Theta + 3$ °C), at $\phi_b = 1.5 \times 10^{-5}$. The dash–dot (– · –) curve and the dashed curve (- - -) are based on the corresponding calculated curves, for PS1 and PS5 respectively, with the force and separation axes multiplied by the same factors α and β as in Figure 13.

curves superposed on the data. We note the rather good qualitative fit, especially in the high-repulsion regime. In particular, we note that scaling the calculated PS1 profile using the same multiplicative factors α and β results in a very reasonable agreement with the data. There is an attractive minimum in the calculated curves which is more marked for PS1 than for PS5. The experimental profiles show no clear indication of such a minimum, though the scatter in the data may mask this to some extent.

It is also of interest to calculate the surface excess for the PS–CP system. It is simple to show that the amount of polymer m adsorbed per unit area is given by[25]

$$m = M\Gamma/6N_A R_g^2 \qquad \text{(VI.2)}$$

where N_A is Avogadro's number. The only direct adsorbance measurement[23] for the PS–CP–mica system is for PS1 ($M = 6 \times 10^5$) and $\phi_b = 1.5 \times 10^{-5}$ at 23 °C. Using $w = 1.0$ and $\sigma = 0.27$, we calculate $\Gamma = 0.93$ (for $w = 1$, $\sigma = 0.27$). This gives $m \simeq 0.4$ mg m^{-2}, compared with the rather "noisy" experimental estimate[23] $m = 2.5 \pm 1.5$ mg m^{-2}. We note that for the $T < \Theta$ calculation[25] a similar underestimation of calculated relative to experimental adsorbance was found. However, in comparing the *ratio* of the adsorbed amounts m(PS1) and m(PS5) for PS1 and PS5, respectively, for the PS–CP–mica system (rather than their absolute values), we find much better agreement. Thus from Table I (items a and e).

$$(m(\text{PS5})/m(\text{PS1}))\ (\equiv \Gamma_0(\text{PS5})/\Gamma_0(\text{PS1})) \simeq 1.35$$

both for adsorbance at 23 °C, from a solution with $\phi_b \simeq 1.5 \times 10^{-5}$. Calculating the surface excess values for $N = 2 \times 10^4$ and $N = 6 \times 10^3$, for $\phi_b = 1.5 \times 10^{-5}$, $w = 1.0$, and $\sigma = 0.27$, we find a ratio

$$\Gamma_0(N = 2 \times 10^4)/\Gamma_0(N = 6 \times 10^3) = 1.36$$

essentially identical with the experimental ratio.

VII. Discussion and Concluding Remarks

In addition to a more general consideration of our model, two main aspects of the comparison of our calculated results with the experimental data deserve comment. The first is that the main qualitative features of interactions between polymer bearing surfaces near $T = \Theta$ are well accounted for, as shown in Figures 12–15; moreover, the relative behavior at different values of the surface excess and molecular weight are correctly (quantitatively) predicted. The second aspect concerns the real discrepancy that emerges when comparing absolute values of the range and magnitude for the experimental and calculated interactions and also of the surface excess. Thus the calculated depth of the attractive well at $\Gamma < \Gamma_0$ is a factor of ca. 2.5 too low, while the range of the calculated interactions is a factor of ca. 4 too low (i.e., the factors $\alpha = 2.4$ and $\beta = 3.8$ in Figures 13–15). The calculated surface excess values are also too low by similar factors when compared with the experimentally estimated adsorbance (though the latter has considerable scatter).

It is of interest to consider the reasons for these discrepancies. Within the framework of the present calculations, a number of factors may be responsible for the differences between calculations and experiment. Our estimates for w and σ (though based on the experimental trends) may be incorrect. (The latter, especially, could well be higher than 0.27 for the PS–CP system: this is because the 20% reduction in Γ corresponding to a 10^4 dilution, which was used to estimate σ, may be due to a much greater dilution in practice. The reason is that, at these dilutions, residual polymer in the solution may adhere to the vessel walls, resulting in substantially lower effective bulk volume fraction. Such a tendency would lead to a higher σ). Another consideration is that the experiments were carried out a little above Θ ($T = \Theta + 3$), so that a small positive *second* virial coefficient should be included in the energy equations in our model. We are currently investigating the incorporation of these modifications in our calculations.

A less likely candidate for the cause of the disagreement between calculations and experiment in terms of absolute quantities may be our choice of N as the number of styrene monomers on the real polymer (so that a polystyrene molecule with $M = 2 \times 10^6$ (PS5) corresponds to $N = 2 \times 10^4$). An argument may be made for using lower N values (with appropriate rescaling of the length a), but, as the size of the styrene monomers and solvent molecules is similar, this argument is not compelling. In any case, lower N values would increase the discrepancy we are attempting to account for.

There are also more fundamental considerations. At

essentially a virial expansion, valid at low ϕ values. Nonetheless, we have used it (in order to take advantage of the additional freedom that an adjustable third virial coefficient bestows, as suggested by experiment[11]) at all ϕ values encountered, up to $\phi = \phi_s^0$ at the wall. As indicated in eq II.13 and also Figure 1, this is of order σ for the single-plate case (at low incubation concentration) and increases on compressing the plates, so that for finite σ values (on the order of 0.3) the low ϕ requirement is not strictly obeyed at all z values. One possibility would be to use the full Flory–Huggins (F–H) expression (this fixes $w = 1$, but see later comments).

Another possible modification, noted earlier,[25] is to recognize that the term in w in eq II.1 is related to the probability of three-segment interactions and at appreciable ϕ values should be modified (in a nonlattice treatment such as ours) to take account of real van der Waals volumes (e.g., by setting $w\phi^3$ as $w(\phi/(1-\phi))^3$. This would prevent the (obviously unphysical) appearance of volume fractions ϕ exceeding unity (including ϕ_s^0) for $\sigma > 1$ and at high plate compressions.

We have also omitted in our equations (eq II.3 for example) any but the leading term $-\gamma_1\phi_s^0$ from the polymer–surface interaction. For cases where the surface volume fraction $\phi_s^0 \not\ll 1$, a second term of the form $(1/2)\gamma_2\phi_s^{0\,2}$ should be included. This would account for correlations (at a mean-field level) between monomers on the surface. Limited calculations incorporating such a term, with a range of γ_2 values up to $0(\gamma_1)$, indicate that no new qualitative features emerge. To a good approximation, including a γ_2 term reduces the surface excess and modifies the two-plate interaction in the same way as would be achieved using only the $-\gamma_1\phi_s^0$ term but with a lower effective value of γ_1. Finally, as noted in section V, the appearance of very large spatial variations in ϕ in the immediate vicinity of the wall may be inadequately modeled using the Cahn–Hilliard formalism, unless higher order terms in the gradient of ϕ are included.

It is also of interest to compare our calculations with other theoretical models. The only comparable detailed calculations are those by Scheutjens and Fleer (SF), whose highly numerical approach uses a mean-field lattice model with effectively the full Flory–Huggins energy of mixing.[3] We have not carried out an exhaustive comparison, though many of their results appear similar. Looking in more detail at a specific case[31] shown by SF, for N [r in their model] = 10 000, Γ [$\theta^t/2$] = 2.5, under Θ conditions [$\chi = 0.5$] and ϕ_b [ϕ^*] = 10^{-6}, they find an interaction profile with (1) an attractive tail at large surface separations, (2) an interaction minimum at a surface separation equivalent to around $0.6R_g$, and (3) a final repulsive wall as the surfaces are compressed (with the profile crossing zero interaction at surface separation $\sim 0.5R_g$). The strength of the interaction at the minimum is estimated by SF (based on available data) to be around 1 order of magnitude lower than experiment. These features are rather similar to our calculations: for example, from Figure 9A we have for N = 10 000, Γ = 2.2 (see curve (b) on Figure 9A and Figure 4 for $\phi_b = 1.5 \times 10^{-5}$) and for Θ conditions (with $w = 0.2$): (1) an interaction profile with an attractive tail at large surface separation, (2) an interaction minimum at a surface separation around $0.5R_g$, and (3) a final repulsive wall as the surfaces are compressed. The small differences in spatial scales are almost certainly due to the slightly different adsorbance values (which themselves depend on the surface coupling in both models). The strength of the interaction at the minimum in our case is a factor of 2.5 lower than the experimental value as discussed earlier, closer to experiment than the "order of magnitude" estimated by SF,[33] though such comparisons are tentative in view of the possible differences in other parameters. What the comparison does clearly show, however, is that the lattice method of SF[3] appears to exhibit very similar discrepancies when compared to experiments as does the present analytical, continuum approach.

In conclusion, we have presented mean-field calculations based on the Cahn–de Gennes formalism,[6,7] and extending our own earlier calculations, for adsorption and interactions between surfaces with adsorbed polymer in Θ conditions. The treatment can be taken a long way analytically and hence gives insight into the role of the various physical parameters of the model. The final numerical calculations are relatively rapid. A detailed comparison with model experiments shows very good qualitative agreement between calculated and observed features of the interaction. In absolute quantitative terms the calculated spatial scales and energy scales are compressed by factors of 3.8 and 2.4, respectively, relative to the measured values. Possible reasons for this have been considered, and we are currently attempting to improve the model to take account of these.

Acknowledgment. We thank the Minerva Foundation, the Israeli Academy (Basic Research Division), the U.S.–Israel Binational Science Foundation, and the Department of Energy (P.P.) under Grant DE-FG03-87ER45288 for their support of this work.

Appendix

We estimate the adsorbances Γ corresponding to the undersaturated profiles presented in ref 23. (In these experiments, direct adsorbance measurements were made only for incubation to equilibrium with the plates far apart.) Examining the strongly repulsive part of each profile, which arises at high compressions (small h), we assume that the interaction results from the osmotic pressure of an essentially uniform concentration of polymer in the gap, $\phi = \Gamma a/h$.

At $T = \Theta$, the osmotic pressure, $\Pi \equiv \phi^2(\partial/\partial\phi)(F/\phi)$, obtained from the Flory–Huggins free energy (eq II.1), is

$$\Pi = T/a^3[(\phi/N)\ln\phi + (1/3)w\phi^3] \qquad \text{(A.1)}$$

For small h, the second term dominates, leading to eq III.11. The interaction energy is given by

$$\gamma(h) = -\int_\infty^h \Pi(h')\,dh' \simeq (wT/6)(\Gamma^3/h^2) \qquad \text{(A.2)}$$

If we now choose a fixed value of the interaction energy, say γ_c, then Γ is related to the half-separation h_c at which $\gamma(h_c) = \gamma_c$, by

$$\Gamma \propto h_c^{2/3}$$

Thus the adsorbances for the undersaturated profiles may be estimated by comparison with the saturated profiles, for which absolute Γ values are available. This is done in Table I for the data of ref 23. We note that the uniform concentration in the gap $2h_c$ corresponding to the measured equilibrium adsorbance of PS1 (Table I) is around $\phi \simeq 0.2$, justifying the neglect of the logarithmic term in eq A.1.

References and Notes

(1) Napper, D. H. *Polymeric Stabilisation of Colloidal Dispersions*; Academic Press: London, 1983.

References and Notes

(1) Napper, D. H. *Polymeric Stabilisation of Colloidal Dispersions*; Academic Press: London, 1983.
(2) (a) Vincent, B. *Adv. Colloid Interface Sci.* **1974**, *4*, 193. (b) Vincent, B.; Whittington, S. G. *Surf. Colloid Sci.* **1982**, *12*, 1.
(3) Scheutjens, J. M. H. M.; Fleer, G. *Macromolecules* **1985**, *18*, 1882.
(4) Rubin, R. J. *J. Chem. Phys.* **1965**, *43*, 2392. DiMarzio, E. A.; Rubin, R. J. *J. Chem. Phys.* **1971**, *55*, 4318.
(5) See: de Gennes, P. G. *Scaling Concepts in Polymer Physics*; Cornell University Press: Ithaca, NY, 1979.
(6) de Gennes, P. G. *Macromolecules* **1981**, *14*, 1637; **1982**, *15*, 492. See also recent work along these lines by: Rossi, G.; Pincus, P. *Europhys. Lett.* **1988**, *5*, 641.
(7) Cahn, J. J. *J. Chem. Phys.* **1977**, *66*, 3667.
(8) de Gennes, P. G.; Pincus, P. *J. Phys. Lett.* **1983**, *44*, L241. Eisenriegler, E. *J. Chem. Phys.* **1983**, *79*, 1052.
(9) Eisenriegler, E.; Kremer, K.; Binder, K. *J. Chem. Phys.* **1982**, *77*, 6296.
(10) Ober, R.; Paz, L.; Taupin, C.; Pincus, P.; Boileau, S. *Macromolecules* **1983**, *16*, 50.
(11) DiMeglio, J. M.; Ober, R.; Paz, L.; Taupin, G.; Pincus, P.; Boileau, S. *J. Phys. Paris* **1983**, *44*, 1035.
(12) Stromberg, R. R.; Tutas, D. J.; Passaglia, E. J. *J. Phys. Chem.* **1965**, *69*, 3955. Takahashi, A.; Kawaguchi, M.; Hiruta, H.; Kato, T. *Macromolecules* **1980**, *13*, 884.
(13) Charmet, J. C.; de Gennes, P. G. *J. Opt. Soc. Am.* **1983**, *73*, 1777. Kawaguchi, M.; Takahashi, A. *Macromolecules* **1983**, *16*, 1465.
(14) Allain, D.; Ausserre, D.; Rondelez, F. *Phys. Rev. Lett.* **1982**, *49*, 1694.
(15) Cosgrove, T.; Crowley, T. L.; Vincent, B. In *Adsorption from Solution*; Rochester, S., Ottewill, R., Eds.; Academic Press: London, 1983.
(16) Cabane, B.; Duplessix, R. In *Colloidal Particles—Polymer Adsorption and Steric Stabilization*; ACS Symposium Series; Goddard, D., Vincent, B., Eds.; American Chemical Society: Washington, DC, 1983.
(17) Tabor, D.; Winterton, R. H. S. *Proc. R. Soc. London* **1969**, *A312*, 435. Israelachvili, J. N.; Tabor, D. *Prov. R. Soc. London* **1972**, *A331*, 19.
(18) Israelachvili, J. N.; Adams, G. *J. Chem. Soc., Faraday Trans. 1* **1978**, *74*, 975.
(19) Klein, J. *Nature* **1980**, *288*, 248. Klein, J. *J. Chem. Soc., Faraday Trans. 1* **1983**, *79*, 99.
(20) (a) Klein, J.; Luckham, P. F. *Nature* **1982**, *300*, 429. (b) *Macromolecules* **1984**, *17*, 1041.
(21) Luckham, P. F.; Klein, J. *Macromolecules* **1985**, *18*, 721.
(22) Israelachvili, J. N.; Tirrell, M.; Klein, J.; Almog, Y. *Macromolecules* **1984**, *17*, 204.
(23) Almog, Y.; Klein, J. *J. Colloid Interface Sci.* **1985**, *106*, 33.
(24) Klein, J.; Pincus, P. *Macromolecules* **1982**, *15*, 1129.
(25) Ingersent, K.; Klein, J.; Pincus, P. *Macromolecules* **1986**, *19*, 1374.
(26) See for example: Reference 5; Chapter III.
(27) Edwards, S. F. *J. Phys.* **1975**, *A8*, 1670.
(28) In the calculations of ref 25, for polymer adsorbed at $T < \Theta$, the surface coupling constant was defined as $\sigma' = (6\gamma_1 a\xi/T)$, where ξ is the Edwards correlation length on the coexistence curve at $\phi = \phi_{eq}$ at the temperature T ($<\Theta$). This converts[25] to $\sigma' = (4\gamma_1 a^2/\upsilon\phi_{eq}T)$ where $-\upsilon$ is the (negative) second virial coefficient at $T < \Theta$. For polystyrene at 24 °C, $\upsilon \simeq 0.2$ and $\phi_{eq} \simeq 0.3$, so that for our definition $\sigma = (6\gamma_1 a^2/w^{1/2}T) \simeq (0.1/w^{1/2})\sigma'$. Thus, assuming that γ_1 is insensitive to temperature, the midrange value of $\sigma' = 3$ used in ref 25 corresponds to $\sigma = 0.6$ for $w = 0.2$, as indicated in the text. This is not necessarily a good assumption since near $T = \Theta$ changes in temperature also change υ, and thus the energy balance determining γ_1.
(29) Terashima, H. *J. Colloid Interface Sci.* **1987**, *117*, 523.
(30) The experiments on PS1 and PS2 were carried out under slightly different conditions, in different laboratories,[22] and so cannot be strictly compared with each other quantitatively. Both, however, are expected to show similar trends.
(31) See ref 3, Figure 8a,b.
(32) See Figure 3 of ref 25. We note that in ref 25, Γa^2 was defined as equivalent to the present Γ_0. We also note that the calculated adsorbances in ref 25 for $T < \theta$ are quite sensitive to the values of the experimental parameters used in their calculation.
(33) However, a detailed examination of the SF profiles for the case considered suggests that their energy scale is too small by about a factor of 3.5 when compared with experiment, rather than their more pessimistic estimate.
(34) Note added following submission: the PS–CP system was also studied very recently by: Hu, Y.-W.; Van Alsten, J. Granick, S. *Langmuir* **1989**, *5*, 270.

Registry No. PS, 9003-53-6.